DESIGN AND EVALUATION OF A 200 N HYNOX THRUSTER CONTROL ALGORITHM IN A HARDWARE IN THE LOOP SIMULATION OF A LANDING DEMONSTRATOR

BARI, ITALY | 18 – 21 MAY 2026

Fabio Addario(1), **Till Hörger**(1), **Marc Gritzka**(2), **Christoph Kirchberger**(1), **Stephan Schlechtriem**(1)
(1) *German Aerospace Center - DLR, Institute of Space Propulsion, Lampoldshausen, Germany,*
Email: fabio.addario@dlr.de
(2) *InSpacePropulsion Technologies GmbH, Ludwigsburg, Germany*
Email: marc.gritzka@isptech.de

KEYWORDS: Chemical Rocket Propulsion, Green Propellants, HyNOx, Nitrous Oxide, Thrust Control, Control Algorithms, Satellite Propulsion, Hardware in the Loop, Lander, Hopper

ABSTRACT:

At the German Aerospace Center's (DLR) facility in Lampoldshausen research on less expensive alternatives for hydrazine as rocket propellant is conducted. The propellant combination of nitrous oxide (N_2O) and ethane (C_2H_6) is considered as such. Currently, tests on rocket engines using those propellants are conducted to evaluate their performance. Furthermore, a free flight landing demonstrator for research on planetary soft landings is developed at DLR. Using green propellants and advanced control algorithms, a 30 s flight is to be demonstrated. In this publication, the feasibility of a main engine thrust controller for a 200 N thruster using gaseous nitrous oxide and ethane shall be investigated.

A control valve is inserted into the ethane and nitrous oxide feeding line on the existing M11.5 test bench. then, a control algorithm is developed. It uses using model-based feed-forward control to enable a quick response time. Furthermore, A internal engine model in conjunction with a proportional-integral controller is implemented to enable precise control behavior. To prove feasibility, a hardware in the loop simulation is conducted, where combustion chamber pressure measurements are fed into a flight simulation with internal flight controller. The flight controller then computes a desired thrust value based on the lander's flight state inside the simulation and forwards it to the test setup, where the thrust controller follows this value in a thruster hot fire test. Analysis of these simulation tests conclude a feasible control behavior of the control circle regarding a free flight demonstration.

1. INTRODUCTION

On February the 22nd in 2024, the US-based company *Intuitive Machines, Inc.* succeeded to touch down softly on the moon with their *Odysseus* lander as the first private company to do so [1]. Prior attempts by other companies such as *SpaceIL*, *ISpace Inc.* or *Astrobotic Technology Inc.* have all failed, implying the technical difficulty in archiving robotic lunar soft landings [2], [3], [4].

Since the late 2010s, renewed interest has risen on lunar soft landings [5]. Especially the National Aerospace Administration (NASA) is funding private companies to develop systems for freight transport to the lunar surface via its *Commercial Lunar Payload Services* program. Furthermore, national space agencies from China and India succeeded at touching down softly on the moon in recent years [6], [7]. In Europe, development of the robotic freight transport lander *Argonaut* is conducted to supplement the *Artemis* program [8]. To simulate missions with human lunar operations the *Luna* facility at the DLR in Cologne was established [9]. At DLR in Lampoldshausen control tests with an Apollo-like descent thrust trajectory using a liquid upper stage demonstrator were conducted [10]. To improve a landing system's chance of success, the system needs to be tested on the ground on earth [6]. Thus, at the DLR facility of Space Propulsion in Lampoldshausen, a lander demonstrator using so called green propellants is developed to conduct test flights on earth so advanced control algorithms and actuators can be evaluated.

1.1 The Rocket-Propelled Flight Demonstrator "*The LÄNDer*"

In this project, a testing platform is consecutively assembled and tested until a free flight is possible. In Fig. 1, the current free flight demonstrator CAD model is shown. First, *Merz* established a 1 degrees of freedom (DoF) testbench and simulated a soft landing using a nitrogen cold gas thruster system using mainly PID-based control [11], [12]. *Bischof* developed a reinforcement learning based attitude control algorithm and conducted tests on a 2 DoF nitrogen cold gas test platform [13]. Then the platform was expanded to facilitate tests using HyNOx thrusters. *Schütz* developed a Model Predictive Control algorithm and conducted tests on the aforementioned platform, as shown in Fig. 2 [14]. It shall also be mentioned that *Hörger* is conducting research on a reinforcement-learning-based thrust controller for a 22 N nitrous oxide and ethane gaseous phase fed bipropellant thruster, but outside the *LÄNDer* project [15], [16], [17].

1.2 HyNOx-Propellants

Currently hydrazine-based propellants are widely used in spacecraft propulsion systems. Their hypergolic properties with e.g. dinitrogen tetroxide, high specific impulse and heritage are some of the reasons that make it attractive for propulsion systems. However, its high toxicity and carcinogenic properties cause high

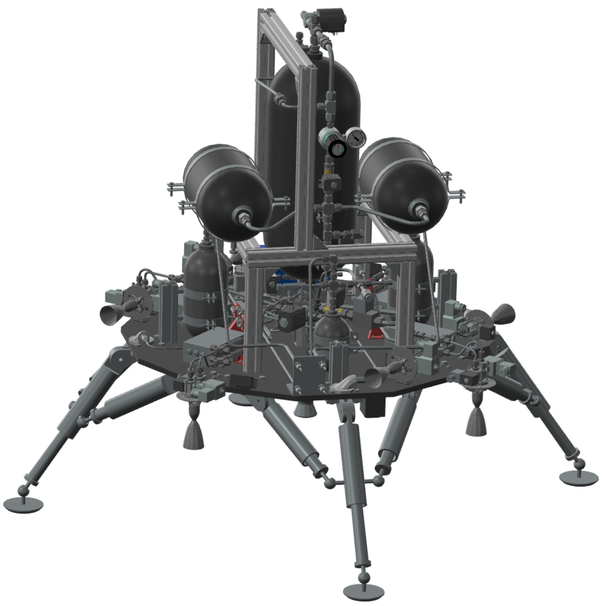

Figure 1: Current lander design model.

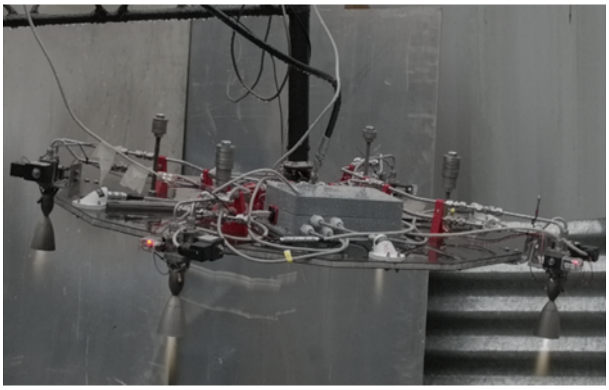

Figure 2: Attitude control test in December 2023 [14].

Figure 3: HyNOx bipropellant thruster family [18]. From left to right: 1 N thruster, 5 N thruster, 22 N thruster and 200 N thruster.

cost during ground operations [19]. Therefore, research on less toxic options, the so-called green propellants, is conducted in the DLR facility of space propulsion among others [20]. Hydrocarbons as fuel and nitrous oxide as oxidizer are commonly known as HyNOx propellants. These pose a viable alternative to hydrazine monopropellant systems for small satellites and CubeSats where minimal system complexity and low cost are required. Due to the propellant's high vapor pressure no pressurization system is needed thus lowering complexity [21]. Ethane has shown to be a suitable fuel in conjunction with nitrous oxide in a bipropellant system [22]. In the DLR institute of space propulsion thrusters in different thrust levels have been developed and are now sold by the DLR spin-off *InSpacePropulsion Technologies GmbH* [18], [23]. These thrusters are shown in figure Fig. 3.

1.3 Course of Action

In this work, the gaseous phase fed 200 N thruster was chosen to facilitate the control algorithm development to lay the ground work for a pressurized liquid propulsion system to be used later as the lander's main propulsion system. To enable control testing, control valves are inserted into the existing 200 N HyNOx test bench. After characterizing the system's response to step inputs by determining mass flow and pressure by generating state space model constants, a thrust control algorithm is designed in a state space model. The control algorithm is then tested on the test bench receiving step inputs and a thrust trajectory generated by a rigid body flight simulation. To verify if the control algorithm's characteristics are sufficient for flight, the measured thrust is fed into a flight simulation where the flight state and flight controller is simulated. The flight controller then calculates a desired thrust which is then fed into the thrust control algorithm, thus archiving a hardware-in-the-loop (HiL) simulation for the thruster and the trust control algorithm.

2. 2. THEORETICAL BACKGROUND

In this section the fundamentals in rocket propulsion and time-discrete control theory are explained.

2.1 Rocket Propulsion

Rocket engines generate thrust by ejecting high velocity gas flow, as is described in Eq. 1.

$$F = \dot{m} \cdot c_e \qquad \text{Eq. 1}$$

At a given mass flow $\dot{m}$, thrust F can be maximized by optimizing the effective exit velocity c_e. In chemical bipropellant propulsion, c_e is largely dependent on combustion chamber pressure, nozzle expanion ratio, molecular weight of the exhaust gases and the oxidizer-fuel mixture ratio ROF. E.g. the maximum value for c_e with nitrous oxide and ethane can be reached at a mixture ratio of $ROF_{opt} = 7.1$ in an vacuum. This can be calculated using NASA's chemical equilibrium with applications (CEA) software [24].

Pressure loss caused by friction and incomplete combustion have negative effects on c_e. The specific impulse is usually used to compare rocket engines and defined by dividing the effective exit velocity by the gravitational acceleration on the earth's surface g as described in Eq. 2.

$$I_{Sp} = c_e/g \qquad \text{Eq. 2}$$

Because of atmospheric pressure thrust is usually lower on earth. Thus I_{Sp} can be increased by increasing the combustion chamber pressure p_{cc} relative to the ambient atmospheric pressure p_{amb}. If an engine's nozzle expansion ratio exceeds the aligned expansion ratio under a given pressure, a significant loss in thrust and I_{Sp} occurs [25], [26], [27], [28].

2.2 Time-Discrete Control Theory

The objective in tracking control is to track a given input signal w. A plant dynamic generates an output signal y. This signal is then subtracted form a desired input signal. This difference is called the control deviation signal e and is the input to a controller. Its purpose is to generate a control output signal u which is fed into the plant in order to minimize the control deviation. Typically, the control loop tracks its desired signal with some delay. Otherwise, the control loop would be non-causal. A typical control loop is shown in Fig. 4. To evaluate the control loop's performance, a transfer

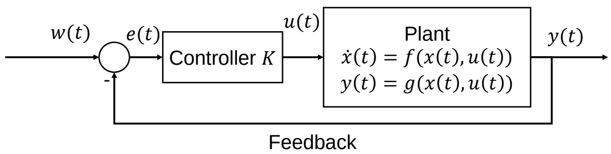

Figure 4: Simplified control loop.

function can be generated through a Laplace transformation of the systems' differential equation if both controller and plant can be assumed as the linear systems $K(s)$ and $G(s)$ respectively. With Eq. 3, the transfer function of the closed loop is given.

$$T(s) = \frac{G(s) \cdot K(s)}{1 + G(s) \cdot K(s)} \qquad \text{Eq. 3}$$

To achieve tracking control using digital computer hardware, the control loop is usually regarded as time-discrete, where the plant state is observed in subsequent points in time separated by the sampling period Δt. This discrete sampling leads however to a loss of information and a delay compared to a continuous loop. To evaluate the control loop's performance the continuous transfer function in Eq. 3 can be transformed using the Tustin formula given in Eq. 4. Thus, the poles of the discrete transfer function can be used to determine whether the control loop is asymptotically stable. If the absolute value of each pole is within the unit circle, the system is asymptotically stable [29], [30].

$$s = \log(z)/\Delta t \approx \frac{2(z-1)}{\Delta t(z+1)} \qquad \text{Eq. 4}$$

3. EXPERIMENTAL SETUP

In this section, the mechanical setup of the propellant feed lines is explained first. Then emphasis is put on the thruster used for the experiments. Lastly, the HiL setup is explained.

3.1 Test Bench

On the M11.5 test bench, gaseous phase fed HyNOx thrusters of varying sizes can be tested under atmospheric conditions [31]. The propellant feedline pressures are set via pressure regulators. Mass flow is measured by coriolis mass flow sensors. The main flow control seat valves are used for the timing during ignition. To undertake thrust control experiments, control valves have been installed into the test bench as depicted in Fig. 5, where the piping and instrumentation diagram is shown. A stepper motor actuated ball valve and a servo motor-controlled seat valve are used in the N_2O and the C_2H_6 lines respectively.

3.2 The IDENO-200B Thruster

The thruster itself is a gaseous phase fed HyNOx thruster, designed to provide 200 N of thrust under vacuum conditions [23]. The combustion chamber is manufactured from Inconel 718 using the selective laser sintering (SLS) technique. During operation, it is regeneratively cooled by its oxidizer N_2O. A small glow plug is used, so the thruster can be ignited multiple times without maintenance. Tests have shown remarkable combustion efficiencies up to 97 % [32]. It should be mentioned that the nozzle flow is usually separated during atmospheric testing due to its large expansion ratio vacuum-optimized nozzle and low operating combustion pressure. This results in significant loss of thrust and specific impulse during firing [25].

3.3 HiL Simulation

In order to verify flight critical components without risk of loss of the entire vehicle, a HiL simulation can be set up. Critical components such as computational hardware, control software and/or actuators exchange data with a flight simulation software in real time. If an error or a bug occurs, the simulated vehicle crashes only inside the simulation instead of damaging real flight hardware, thus reducing development cost [33], [34].
To optimize and verify the lander's design, a custom made 6 DoF flight simulation was set up. Its purpose is to prove that the design and flight controller is viable under perturbations such as aerodynamic forces, thruster transients, model deviations and main engine misalignment as well as the conjunction of different control loops. Some of the used simulation parameters are given in Tab. 1.

To verify whether the discussed thrust controller is viable, the flight simulation was adapted to facilitate a HiL simulation. the HiL setup described in this paper is depicted in Fig. 6. It is set up as follows: the engine's thrust is calculated from combustion chamber pressure measurements and fed into the flight simulation, where the simulated lander' flight state is updated.

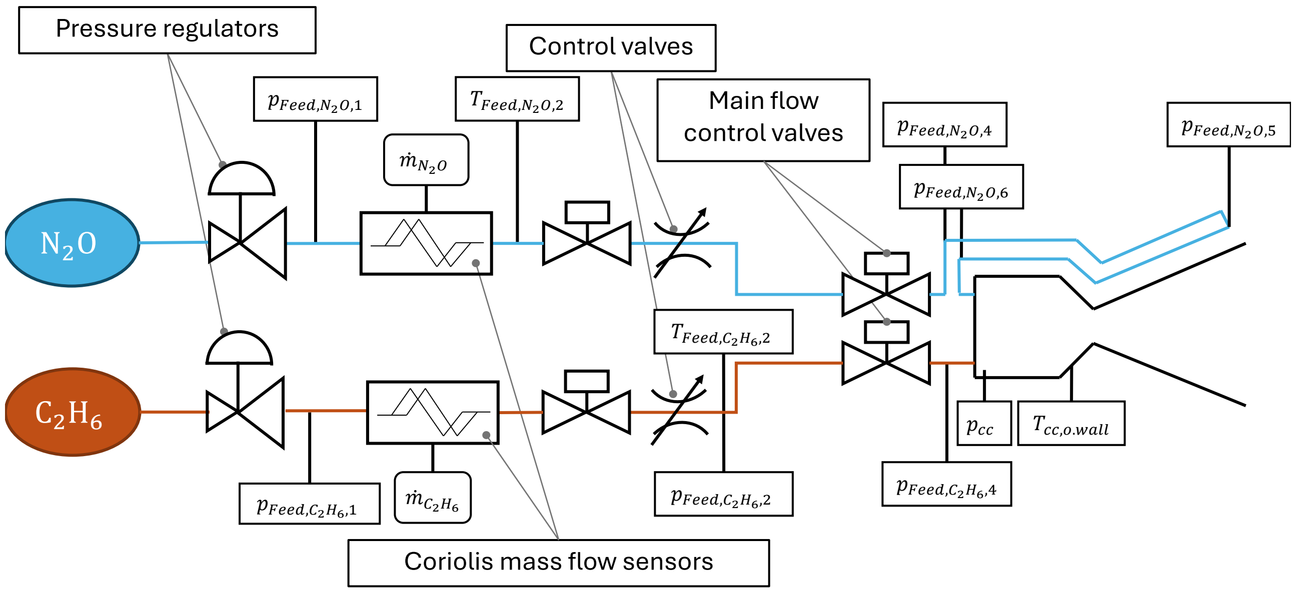

Figure 5: Test bench setup at M11.5 in Lampoldshausen.

Table 1: Selected lander simulation parameters.

Parameter	**Value**
Simulation Time Step	5 ms
Initial mass	45 kg
Flight duration	30 s
Attitude thruster count	8
Thruster maximum thrust	12 N
Thruster minimum impulse bit	0.48 Ns

Based on this flight state, the simulation's internal flight controller calculates the desired value for the attitude control thrusters and the main engine. The main engine desired thrust is then given to the external thrust controller via *Socket* communication. The thrust controller computes desired control valve positions for the test bench. Those then influence the main engine's thrust on the test bench thus forming a closed control loop with the simulation. As a single 200 N engine does not provide enough force for a liftoff on earth under the parameters given in Tab. 1, the measured force is amplified by a factor of 8 in the flight simulation. Essentially, this means that a total of 8 main engines are simulated on the lander.

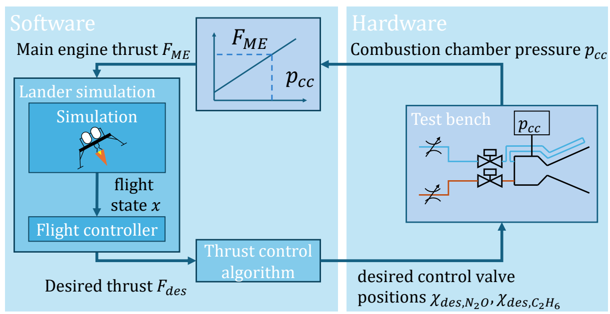

Figure 6: HiL simulation setup.

The simulated waypoint trajectory, that the lander has to follow, consists of three waypoints. The first waypoint is above the starting point in an altitude of 10 m, followed by the second waypoint that is horizontally spaced 31 m away from the first one. The last one leads to a descent to 1 m above the ground. The simulated trajectory is shown in Fig. 7.

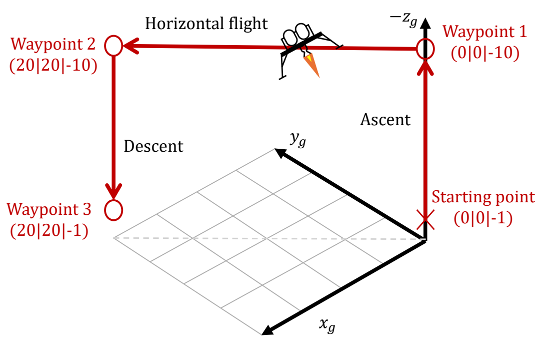

Figure 7: Waypoint trajectory used in the HiL simulation.

The simulation is controlled by cascaded waypoint tracking controller, inspired from multicopter and aircraft flight control algorithms [35], [36], [37]. Each controller block depicted in simply amplifies its control deviation to its input by a proportional gain vector. The only exception is the attitude rate controller as it is an on-off rate controller. the controller structure is shown in Fig. 8.

4. THRUST CONTROLLER

As the proposed thrust controller utilizes model data, first the model identification has been described. Secondly, the controller setup itself is explained. Lastly, the control loop's stability is discussed.

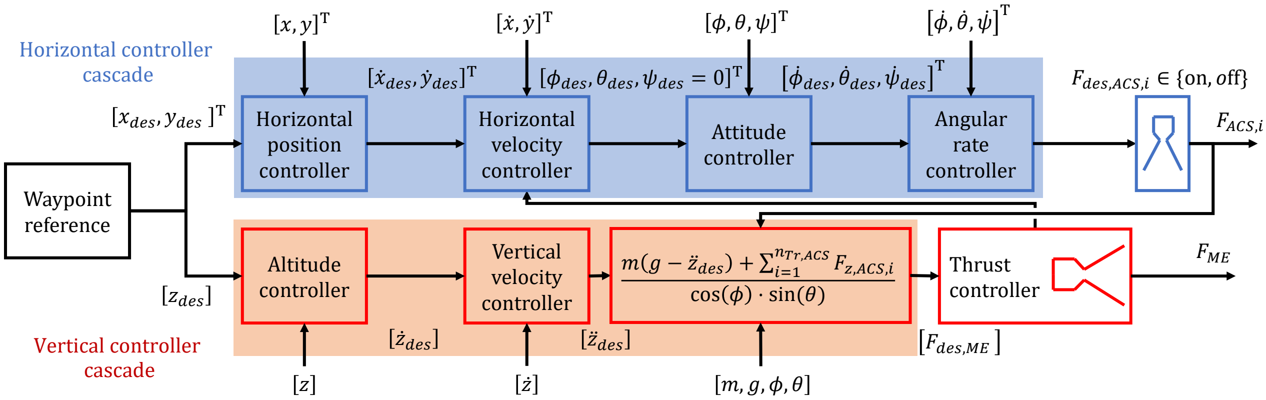

Figure 8: Flight controller used in the HiL simulation.

4.1 Model Identification

Although the objective of the controller is to control thrust, the thrust itself will not be measured and used inside thrust controller if the thruster is installed on a lander. Therefore, the delivered thrust is estimated by using a first-order polynomial $F = P(p_{cc})$ in dependence of the combustion chamber measurement p_{cc}. The used polynomial and the relation between chamber pressure and thrust is shown in Fig. 9. As the polynomial differs significantly from the aligned nozzle flow thrust, it becomes apparent that the nozzle flow during the tests is separated as the thruster is designed with an expansion ration fit for low ambient pressure. The transient behavior of the thruster is mainly dominated by the nitrous oxide control valve. A model using a second order time delay in conjunction dead time is used. Its continuous transfer function $\hat{G}(s)$ is described in Eq. 5, however the controller described in subsection 4.2 and subsection 4.3 uses its Tustin approximation $\hat{G}(z)$ given in Eq. 6. There, the dead time is rounded up to 3 discrete sampling periods Δt.

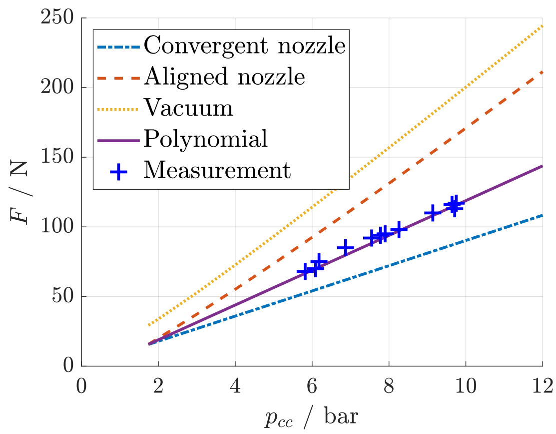

Figure 9: Correlation between thrust and combustion chamber pressure in the used controller.

$$\hat{G}(s) = \frac{e^{T_{dead} \cdot s}}{(T_1 \cdot s + 1) \cdot (T_2 \cdot s + 1)} \quad \text{Eq. 5}$$

$$\hat{G}(z) = \frac{\Delta t^2 (z^2 + 2z + 1)}{z^3 (a_2 z^2 + a_1 z + a_0)} \quad \text{Eq. 6}$$

$$a_0 := \frac{4T_1T_2 - 2\Delta t(T_1 + T_2) + \Delta t^2}{a_2} \quad \text{Eq. 7}$$

$$a_1 := \frac{2\Delta t^2 - 8T_1T_2}{a_2} \quad \text{Eq. 8}$$

$$a_2 := 4T_1T_2 + 2\Delta t(T_1 + T_2) + \Delta t^2 \quad \text{Eq. 9}$$

The model parameters of the second order system T_1, T_2 and the dead time T_{dead} are determined by minimizing the square error of the model deviation to the measurement data of multiple step responses. The results are given in Tab. 2.

Table 2: Plant model parameters.

Parameter	Value
Sampling period	0.1 s
Time constant T_1	0.1438 s
Time constant T_2	0.1790 s
Time constant T_{dead}	0.2664 s

A step response in the continuous plant model and measurement data is shown in Fig. 10.

Lastly, the flow characteristics of the control valves have to be determined. Therefore, the valve is opened at varying valve positions and the mass flow is measured using coriolis mass flow sensors. Using Eq. 10 as the equation for critical flow of an ideal gas through an orifice, a correlation between valve position χ_i and the effective orifice area $A_{eff,i}$ can be determined for N_2O and C_2H_6 respectively [38]. The variables $\dot{m}_i, R_i, T_i, p_{Feed,i}, \gamma_i$ respectively refer to the mass flow, ideal gas constant, fluid temperature, feedline pressure and the isentropic gas constant, to the respective medium i. γ_i is interpolated using the *CoolProp* fluid properties database [39].

$$A_{eff,i} = \frac{\dot{m} \cdot \sqrt{R \cdot T_{Feed}}}{p_{Feed} \cdot \Gamma}, \quad \text{Eq. 10}$$

$$\Gamma = \sqrt{\gamma \left(\frac{2}{\gamma + 1}\right)^{\frac{\gamma+1}{\gamma-1}}} \quad \text{Eq. 11}$$

A 5-order polynomial is fitted through the recorded data to interpolate between the values. It should be noted that Eq. 10 is only valid if $p_{Feed,i}$ is sufficiently lower than the vapor pressure at a given temperature $T_{Feed,i}$. Otherwise, different models provide more accurate results [40], [41], [42].

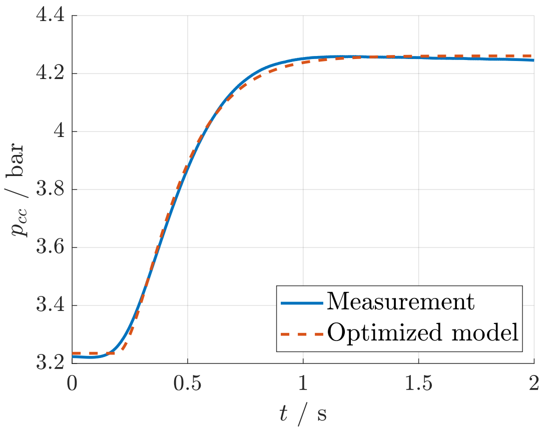

Figure 10: Nitrous oxide valve step response in measured combustion chamber pressure data and PT-2 model.

4.2 Thrust Control Algorithm

As is depicted in Fig. 11, the thrust controller uses a feed forward filter to alter the input signal, similar to [43]. In this work it was used to accelerate the response by amplifying the 1st order time derivative in the desired thrust signal. Using a CEA lookup table, the desired mass flows to achieve the desired chamber pressure can be calculated for a given mixture ratio. There is no feedback loop implemented controlling the mixture ratio. To compensate for deviations in the combustion chamber pressure p_{cc} resulting from errors in the valve polynomials and combustion efficiencies in the CEA lookup table, a proportional-integral (PI) controller is used to eliminate steady-state error. On its own, the PI controller causes overshoots resulting from the plant delay. Therefore, the transient plant model discussed in subsection 4.1 is used to filter the PI controller's input. The controller gains have been determined in a parameter optimization, where the integral of control deviation in multiple step responses with varying model deviation has been used as a loss function.

4.3 Stability

To prove whether the proposed controller is stable during operations, a time discrete state-space model of the control loop is set up in a linear differential equation of the form of Eq. 12 and then transformed into a transfer function using Eq. 13 [29, page 511].

$$\begin{aligned} x_{k+1} &= Ax_k + Bu_k \\ y_k &= Ax_k + Cu_k \end{aligned} \quad \text{Eq. 12}$$

$$G(z) = C(zI - A)B + D \quad \text{Eq. 13}$$

A control loop is considered stable if all poles of the transfer function $G(z)$ are within the unit circle. In Fig. 12 a plot of the poles and zeroes of $G(z)$ is shown for the nominal model as well as a plant deviation of +30 % and -30 %. It is visible, that all poles are within the stability boundary [29]. In Fig. 13 the influence of the model deviation is shown in a step response.

5. Evaluation

Firstly, the thrust control loop is evaluated on its own by reviewing the response to step inputs in the desired value. Then, the HiL performance is regarded by evaluating the performance of the control loop in conjunction with the flight simulation with its flight controller.

5.1 Step Responses

In Fig. 14, test data of step input tests are shown. The control loop is tested with and without the PI-controller. The controller is fed with an input trajectory with multiple steps. It is activated two seconds into the test. During the steps in $t = 20.5$ s and $t = 40.5$ s it becomes apparent that some model deviation in the only-feed-forward controller leads to significant steady-state error. The control loop including the PI controller however quickly converges to the desired value after minor overshoots, thus improving controller performance. Note that in both tests the controller is activated 2 seconds after ignition in $t = 0$ s. In $t = 50.5$ s, the desired value chamber pressure jumps to 8 bar. However, both controllers cannot reach this value. This is due to insufficient feed pressure and has nothing to do with controller performance.
In Fig. 15, the mixture ratio ROF is shown during a controller test with the same step input trajectory as shown in Fig. 12. However, the desired mixture ratio was not altered during tests and set on $ROF_{des} = 25$. The peaks in the recorded data are likely due to differing filter time constants inside the mass flow meters after a jump in the desired chamber pressure $p_{cc,des}$. Especially following $t = 30.5$ s and $t = 40.5$ s some steady state error becomes visible. This likely due to model deviation in the control valve flow model described in 3.1. As installing mass flow meters on a lander platform is deemed unpractical, no feedback of mixture ratio can be implemented. If more accuracy is needed for a flight demonstration (e.g. to limit thermal loads on the chamber wall or to maximize specific impulse), more effort needs to be put on control valve model identification in the future.

6. HiL Tests

In Fig. 16, the altitude states in two HiL simulations are shown. Due to lower initial chamber pressure dur-

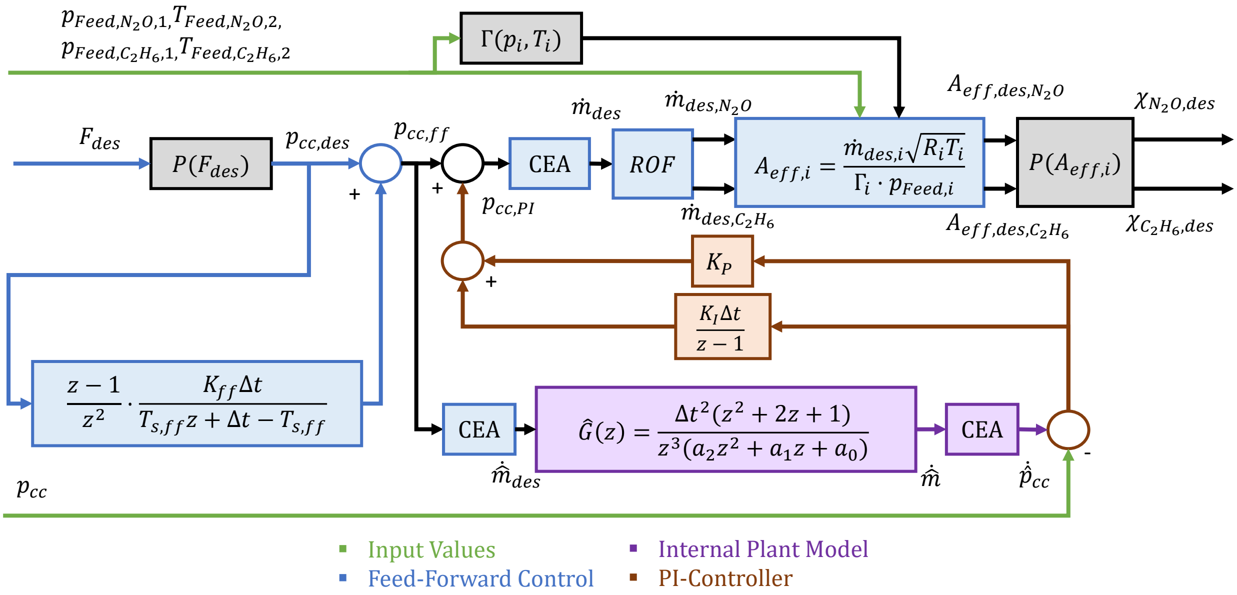

Figure 11: Diagram of the implemented thrust controller.

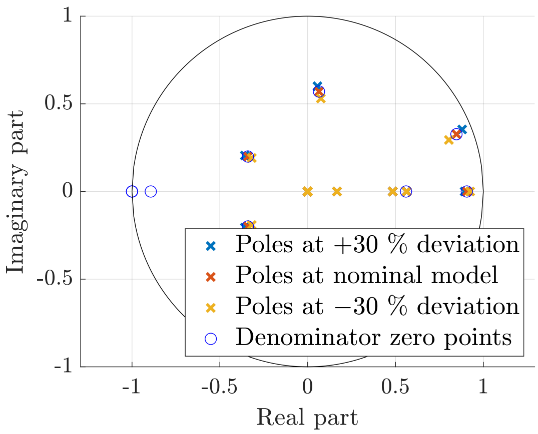

Figure 12: Poles and zeros of the control loop model under different model deviations.

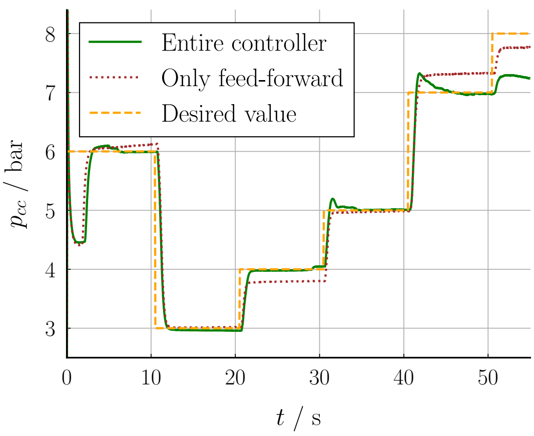

Figure 14: Tracking behaviour of the control loop with and without feedback.

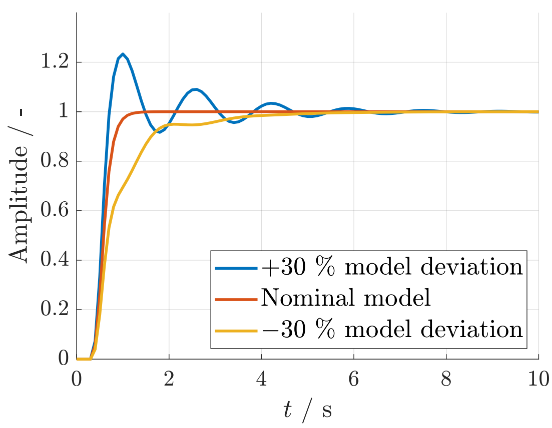

Figure 13: Step response with different model deviations.

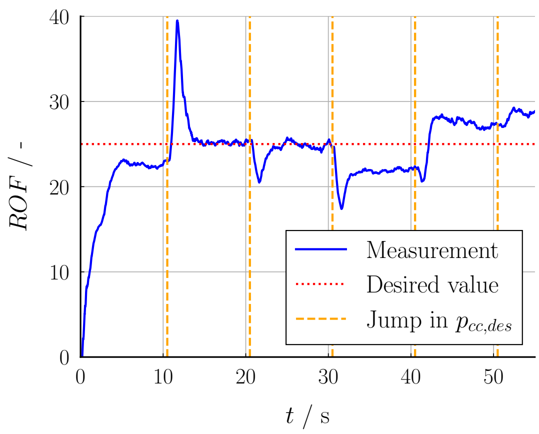

Figure 15: Mixture ratio measurement during a control test.

ing ignition, the altitude decreases during the first two seconds. This however has nothing to do with the controller performance. Both controllers are able to follow their desired value signal. Furthermore, both controllers fall below the 10 m line after $t = 8$ s for a short time since more thrust is needed for horizontal flight. Because of the control loops delay, it can only be provided after the lander starts to tilt to accelerate horizontally. For the same reason both controllers rise above the 10 m mark at $t = 11$ s, because the thrust controller need time to lower its thrust after it is flying straight. The controller without the PI feedback loop shows more deviation and overshoot during flight. Therefore, use of a thrust feedback loop is recommended.
Fig. 17 and Fig. 18 display the thrust and desired thrust signals of the same simulations as described in Fig. 16. It can be observed, how the thruster performs during ignition. The thrust measurement spikes during ignition, which occurs shortly after $t = -2$ s. The thrust however decreases shortly after. This is likely due to the propellants being in equilibrium before the main flow control valves are opened. When the propellant is extracted from the supply during the test, the equilibrium of vapor and gaseous phase cannot be upheld, thus lowering thrust significantly. However, considering the thrust signal for evaluation of the control performance is difficult, since both controllers seem to track their desired values similarly. This implies the benefit of a HiL simulation instead of simply tracking a desired thrust signal because the difference in control quality becomes visible in the altitude plot in Fig. 16.

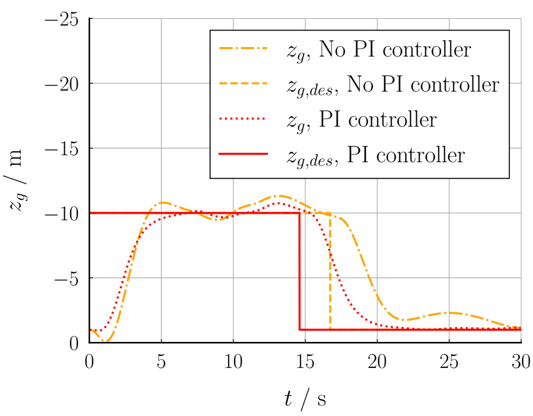

Figure 16: Altitude and desired altitude during simulated flights with different controllers.

7. CONCLUSION

At the DLR institute of space propulsion research is conducted on alternative propellants and their chemical propulsion systems for satellite and planetary lander propulsion. Among others, nitrous oxide and ethane are deemed to be a viable alternative. Additionally, research is conducted on a landing demonstrator which is being developed to conduct test flights on earth. Its purpose is to enable in-flight controller and thruster tests for green propulsion systems to gen-

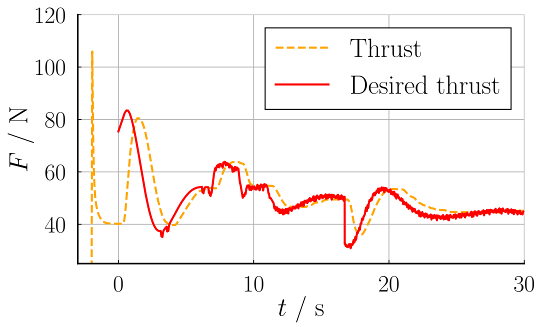

Figure 17: Thrust and desired thrust, corresponding to the tests in Fig. 16 without the PI feedback controller.

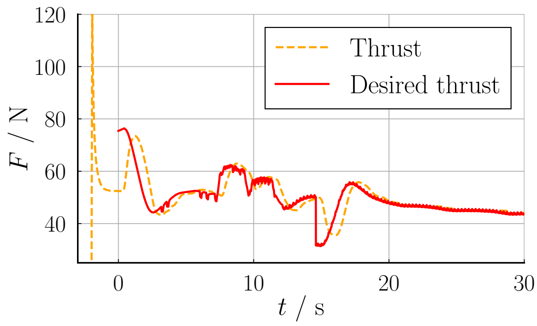

Figure 18: Thrust and desired thrust, corresponding to the tests in Fig. 16 with the PI feedback controller.

erate system understanding.

In this work, a thrust controller is developed for a 200 N gaseous fed nitrous oxide and ethane bipropellant thruster. The controller uses a feed-forward filter and a CEA lookup table to enable a quick response time. To achieve steady state accuracy, a PI controller is fed with the combustion chamber pressure and the desired value filtered by the thruster's transient model.

Hot-fire testing of the control loop shows that it has sufficient response time and low steady state error. To prove the controller's viability in a lander application, a HiL simulation was conducted. In hot-fire tests, thrust measurements were sent to a software flight simulation. There, the flight simulation's flight controller computes a desired thrust signal in real time, which is then fed into the control loop. A PI-feedback-controller has proven better altitude tracking than a similar controller without feedback. It was determined that the thrust control loop's characteristics are suitable for use on a landing demonstrator.

In future, tests will be conducted using liquid fed HyNOx rocket engines. The controller's feed forward filter and gains will likely have to be adjusted while the controller structure is deemed viable.

References

[1] Zajac, M. (2024). *Odysseus Lands on the Moon.*

[2] Shyldkrot, H. et al. (2019). *The first commercial lunar lander mission: Beresheet*.
[3] Banks, M. (2023). "Japanese private craft crash lands on Moon". *Physics World* 366, pp. 11i–11i.
[4] Witze, A. (2024). *Private Moon Lander Dies Before Reaching Lunar Surface: Astrobotic, the US firm that launched the Peregrine craft, says it will learn from missteps.* Nature.
[5] Crawford, I. A. et al. (2012). "Back to the Moon: The scientific rationale for resuming lunar surface exploration". *Planetary and Space Science* 741, pp. 3–14.
[6] Yu, D.-Y., Sun, Z.-Z. & Zhang, H. (2021). *Technology of Lunar Soft Lander*. Springer, Singapore.
[7] Raina, S. & Bhat, K. (2024). "Chandrayaan-3: India's Third Lunar Mission". *International Journal of Science and Research (IJSR)* 1311, pp. 1384–1386.
[8] European Space Agency (2025). *Argonaut: Europe's lunar lander programme*.
[9] Casini, A. E. et al. (2020). "Lunar analogue facilities development at EAC: the LUNA project". *Journal of Space Safety Engineering* 74, pp. 510–518.
[10] Dresia, K. et al. (2025). "Hot-Fire Testing and System Analysis of the LUMEN Liquid Upper Stage Demonstrator Engine". *3rd International Conference on Flight Vehicles, Aerothermodynamics and Re-entry (FAR)*.
[11] Merz, F. (2022). "Fundamental Comparison between Different Thrust-Throttling Approaches and Implementation of Selected Procedures in a 1-DoF-Cold-Flow-Demonstrator". Master's thesis, University of Stuttgart, Stuttgart.
[12] Merz, F. et al. (2023). *Green Propulsion Demonstrator The LANDer*.
[13] Bischof, L. (2023). "Robust Attitude Control System Based on Reinforcement Learning for a Spacecraft Lander Demonstrator". Master's thesis, Rheinisch-Westfälische Technische Hochschule Aachen, Aachen.
[14] Schütz, M. (2024). "Design and Evaluation of an Attitude Control System for a Spacecraft Landing Demonstrator". Bachelor's thesis, Karlsruher Institute of Technology, Karlsruhe.
[15] Hörger, T. et al. (2024). "Experimental and Simulative Evaluation of a Reinforcement Learning Based Cold Gas Thrust Chamber Pressure Controller". *Acta Astronautica* 219, pp. 128–137.
[16] Hörger, T. et al. (2022). "DEVELOPMENT OF A TEST INFRASTRUCTURE FOR A NEURAL NETWORK CONTROLLED GREEN PROPELLANT THRUSTER". *8th Space Propulsion Conference*.
[17] Hörger, T. et al. (2025). "Machine Learning Based Combustion Chamber Pressure and Mixture Ratio Controller - Simulative and Experimental Evaluation of Control Performance". *AIAA Science and Technology Forum and Exposition, AIAA SciTech Forum 2025*.
[18] Werling, L. et al. (2023). "From Lampoldshausen to Orbit: DLR Spin-off GreenDelta and the Development status of Green Propellant Thrusters based on H2O2 and N2O". *Proceedings of the Aerospace Europe Conference - EUCASS - 2023*. CEAS.
[19] Amrousse, R. & Yan, Q.-L. (2024). *Recent Advancements in Green Propulsion: Green Propellants for Micropropulsion Systems*. Springer Nature Switzerland and Imprint Springer, Cham.
[20] Werling, L. et al. (2022). *Research and Test Activities on Advanced Rocket Propellants at the Test Facility M11 and the Physical-Chemical Lab of DLR in Lampoldshausen*.
[21] Sarritzu, A. & Pasini, A. (2024). "Performance comparison of green propulsion systems for future Orbital Transfer Vehicles". *Acta Astronautica* 217, pp. 100–115.
[22] Sarritzu, A. et al. (2024). "Review and perspectives of "Green" Self-Pressurizing Propellants for In-Space Propulsion and their applicability to Orbital Stages". *AIAA SCITECH 2024 Forum*. American Institute of Aeronautics and Astronautics, Reston, Virginia.
[23] InSpacePropulsion Technologies GmbH (2026). *Pioneering a new era of space propulsion*.
[24] Gordon, S. & McBride, B. J. (1994). *Computer Program for Calculation of Complex Chemical Equilibrium Compositions and Applications: I. Analysis*.
[25] Stark, R. (2005). "Flow separation in rocket nozzles, a simple criteria". *41st AIAA/ASME/SAE/ASEE Joint Propulsion Conference & Exhibit*, p. 3940.
[26] Huzel, D. K. & Huang, D. H. (1967). *Design of Liquid Propellant Rocket Engines*.
[27] Sutton, G. P. & Biblarz, O. (2001). *Rocket propulsion elements*. Wiley, New York and Weinheim.
[28] Messerschmid, E. & Fasoulas, S. (2017). *Raumfahrtsysteme: Eine Einführung mit Übungen und Lösungen*. Springer Vieweg, Berlin.
[29] Lunze, J. (2016). *Regelungstechnik*. Springer Vieweg, Berlin and Heidelberg.
[30] Lunze, J. (2020). *Regelungstechnik*. Springer Vieweg, Berlin.
[31] Wilhelm, M. et al. (2019). "Test Complex M11: Research of Future Orbital Propulsion Systems and Scramjet Engines". *70th International Astronautical Congress (IAC)*. International Astronautical Federation, 100 Avenue de Suffren, 75015 Paris, France.
[32] Addario, F. (2025). "Testing of a 200 N thruster and investigation of controllability for utilisation in a landing demonstrator". MA thesis, University of Stuttgart.
[33] Waxenegger-Wilfing, G. et al. (2020). "Hardware-In-The-Loop Tests of Complex Control Software for Rocket Propulsion Systems". *71st International Astronautical Congress (IAC)*. International Astronautical Federation, 100 Avenue de Suffren, 75015 Paris, France.

[34] Bacic, M. (2005). “On hardware-in-the-loop simulation”. *Proceedings of the 44th IEEE Conference on Decision and Control*. IEEE, pp. 3194–3198.

[35] Lestari, D. et al. (2022). “Quadcopter Design With Waypoint Mission Using PID Control System”. *2022 11th Electrical Power, Electronics, Communications, Controls and Informatics Seminar (EECCIS)*. IEEE, pp. 287–291.

[36] Stephan, J. (2025). *Multicopter Flight Control*. Springer.

[37] Lu, P. et al. (2016). “Aircraft fault-tolerant trajectory control using incremental nonlinear dynamic inversion”. *Control Engineering Practice* 57, pp. 126–141.

[38] Shapiro, A. H. (1953). “The dynamics and thermodynamics of compressible fluid flow”. *New York: Ronald Press*.

[39] Bell, I. H. et al. (2014). “Pure and Pseudo-pure Fluid Thermophysical Property Evaluation and the Open-Source Thermophysical Property Library CoolProp”. *Industrial & engineering chemistry research* 536, pp. 2498–2508.

[40] La Luna, S. et al. (2022). “A two-phase mass flow rate model for nitrous oxide based on void fraction”. *Aerospace* 912, p. 828.

[41] Dyer, J. et al. (2007). “Modeling feed system flow physics for self-pressurizing propellants”. *43rd AIAA/ASME/SAE/ASEE Joint Propulsion Conference & Exhibit*, p. 5702.

[42] Waxman, B. S. (2014). *An investigation of injectors for use with high vapor pressure propellants with applications to hybrid rockets*. Stanford University.

[43] Bangura, M. & Mahony, R. (2017). “Thrust control for multirotor aerial vehicles”. *IEEE Transactions on Robotics* 332, pp. 390–405.